SLAC-PUB-1331
(I)
October 1973

REVIEW OF SUB-NANOSECOND TIME-INTERVAL MEASUREMENTS*

Dan I. Porat

Stanford Linear Accelerator Center
Stanford University, Stanford, California 94305

ABSTRACT

A review of time-interval measurements in the sub-nanosecond regime is presented and the various methods are compared as to their precision, stability, resolution, and other essential parameters. Calibration methods, stabilization, and correction for time walk are also discussed.

1. INTRODUCTION

In many physics experiments a need arises to measure short time intervals with good resolution and accuracy. Such experiments are in the area of mean lifetime measurements of excited nuclear states, angular correlation functions, time-of-flight measurements, particle identification, and any nuclear physics experiments in which time information is either essential or auxiliary in reconstructing an event. Particles interacting with matter generate electrical pulses which have to be measured with the best accuracy, stability and resolution consistent with the experimental requirements. The time intervals to be discussed in this paper span six decades being in the range of 10^{-12} to 10^{-6} s although some techniques can easily be adapted to extend the upper limit. Accuracies and resolutions are of the order of 1 percent in most circuits to be discussed; some techniques, however, are capable of higher accuracies and resolutions.

At present the principal limitation in measurement accuracies lies in the transducers such as photomultipliers or semiconductor detectors. The electrical signals generated by these transducers exhibit transition times that are much longer than the accuracies required in many time-interval measurements. The detector is commonly followed by a discriminator-shaper circuit which, ideally, delivers a pulse of standard amplitude, duration, or both once its threshold has been exceeded by the incoming signal. The time definition of the output of such a discriminator-shaper circuit is degraded due to the finite risetime of the incoming signal, and the large dynamic range typical in particle detection. Several schemes have been developed to minimize the timing errors from the above sources and these were discussed in this issue in A. Barna's paper on "Nanosecond Trigger Circuits" and F. Kirsten's paper on "Nanosecond Coincidence Measurements." We can therefore minimize in this paper all discussion pertaining to lack of time resolution resulting from the detector properties and concentrate the treatment on the types of circuits available for short time-interval measurements, their relative merits and limitations and their typical applications.

We shall make a distinction between a systems resolution and the intrinsic resolution of a measurement. The former takes into consideration the contribution to the resolution from all components of the system while the latter is restricted to the resolution of the time-interval measuring machine only.

In the following we describe the principal methods of time-interval measurement:

(a) Time-to-digital converters, TDC's, using counter methods,
(b) vernier techniques,
(c) pulse overlap techniques,
(d) circuits utilizing the start-stop principle, and
(e) picosecond measurements utilizing the RF structure of accelerated particles.

Time scale and time delay calibration are discussed in Section 7. Since many experiments involve accumulation of data over extended period we have included a section (Section 8) on stabilization of time-interval measurements. Finally, in Section 9 we discuss applications and some practical considerations.

2. TIME-TO-DIGITAL CONVERTERS, TDC's, USING COUNTER METHODS

The TDC principle utilizes a gated time-marker generator of a well-defined and stable period T. The generator is gated on by the start pulse and gated off by the stop pulse. A counter records the number n of time markers within the start-stop time interval as shown in Figure 1. The dynamic range of the instrument is large and depends only on the bit capacity of the counter; its integral linearity is very good. The accuracy is defined by the stability of the generator frequency. The time resolution is T and with modern counters having a 500 MHz toggling rate T is thus 2 ns. The resolution of such a TDC may be improved by use of two 500 MHz oscillators that are synchronized to start on opposite phases of the period as shown in Figure 2. A resolution of 1 ns is thus obtained at the expense of using an additional counter.

Further improvements are possible through use of several phase controlled oscillators to obtain a subdivision of the clock period. Thus De Lotto et al. using a 1.25 GHz oscillator achieved a 50 ps resolution at $\sigma = 0.25\%$ by subdividing the period into 16 intervals (Lo 64). These complications in circuitry are justified when a large dynamic range is required. They have been successfully employed in TDC's having a resolution of 1 ns in a range of 2^{17} ns (Me 66).

When the clock frequency is about 100 MHz one can utilize an interpolation circuit to obtain resolutions of about 1 ns. A simplified block diagram of a representative circuit, is shown in Figure 3. Assume that the clock frequency is 125 MHz, i.e., a period of 8 ns. A delay line with taps at 1 ns intervals is inserted in the signal path; each delay tap is connected to a coincidence circuit having 1 ns resolution. Initially the counter starts accumulating counts after the oscillator has been gated by a start pulse. A stop pulse is simultaneously applied to (a) the gated oscillator to stop further oscillations and to (b) the second inputs of all coincidence units. The interpolated time interval thus obtained is encoded and presented as the least significant three bits together with the counter bits.

Interpolation schemes of this type suffer from differential non-linearities which have a periodicity of the oscillator period. Such non-linearities may be minimized using an additional interpolation unit in the stop channel that is incremented modulo n by one unit delay at each measurement, where n is the number of subdivisions. The added delay value at each measurement is digitally subtracted from the number formed by the counter and interpolator outputs to yield the correct result. This statistical equalization of the interpolated time reduces the differential non-linearities to negligible values.

3. VERNIER PRINCIPLE

The vernier principle is illustrated in Figure 4; two clocks of slightly different periods are employed and the

*Work supported by the U. S. Atomic Energy Commission.

(Printed in IEEE Trans. on Nucl. Sci. Vol. NS-20, No. 5, p. 36-51 (1973))

time interval τ to be measured is expanded by a factor k,

$$k = \frac{T_1}{T_1 - T_2} = \frac{T_1}{\Delta T} = \frac{f_2}{f_2 - f_1} = \frac{f_2}{\Delta f} \qquad (1)$$

where

$f_1 = \frac{1}{T_1}$ is the lower oscillation frequency

$f_2 = \frac{1}{T_2}$ is the higher oscillation frequency

Equation (1) can be easily derived from Figure 4 and is valid for $\tau < T_1$. Accuracy and resolution of the instrument can be very high if (a) f_1, f_2 are stable and (b) Δf can be made arbitrarily small. The first condition is easily achievable within the accuracies normally required for short time-interval measurements. However, operation of two frequency sources having a small Δf is possible only with careful shielding, otherwise the oscillators lock into a constant relative phase and have identical periods. A Δf of 1% is usually employed but this figure could be improved. A supervisory circuit is required to prevent inputs to the vernier time analyzer during conversion and for input pulses where $\tau > T_1$.

The block diagram of a typical vernier time interval measurement circuit is shown in Figure 5. The oscillators are gated on by the start and stop pulses, respectively. Since $T_2 < T_1$ the number of accumulated periods in the stop channel gradually catches up with the start channel as shown in Figure 4; when both oscillators are in phase $n_1 = n_2 = n$ and the coincidence circuit delivers an output which gates off both frequency sources at a time $k\tau$

$$k\tau = nT_1 = \tau + nT_2$$

thus

$$\tau = n(T_2 - T_1) = n\Delta T = n\,\frac{\Delta f}{f_1 f_2} \qquad (2)$$

As shown in Figure 5 the measurement employing a vernier type device may be carried out either by measuring the expanded time, $k\tau$, using a relatively slow, time-to-amplitude converter, TAC (see dashed lines) or by counting the periods n until the phases of the two channels are in coincidence (see full lines). The latter method has the advantage that the output is derived in digital form and is therefore compatible with modern data acquisition systems. In either case τ is quantized to time intervals of ΔT duration.

The vernier method may also be used to measure intervals $\tau > T_1$, in which case $n_1 \neq n_2$ and the time expansion, k, derived from the time diagram of Figure 4 is

$$k = \frac{1}{1 - \frac{n_2 T_2}{n_1 T_1}} \qquad (3)$$

As in the case of $\tau < T_1$ two gated oscillators of periods T_1 and T_2 ($T_1 > T_2$) are required having slightly different periods. The start and stop pulses determine the initial relative phases of the oscillators. If the later pulse (stop) is applied to the oscillator having the shorter period the two oscillators will be in phase coincidence after some time during which the start oscillator has completed n_1 periods while the stop oscillator has completed n_2 periods. Two counters are now required to establish the time interval τ under measurement,

$$\tau = n_1 T_1 - n_2 T_2 = (n_1 - n_2)\,T_1 + n_2\,\Delta T \qquad (4)$$

Note that for $\tau < T_1$, $n_1 = n_2$ and Eq. (4) reduces to Eq. (2).

A vernier time-interval digitizer (VTID) utilizing two counters and hence capable of measuring $\tau < T_1$ as well as $\tau > T_1$ is described by Barton and King (Ba 71). The diagram of the instrument that was constructed using MECL II logic is shown in Figure 6 and the timing wave forms in Figure 7. Referring to Figure 6 the circuit may be divided into (a) the supervisory logic (made up of EG&G logic modules) which allows the circuit to operate when the time interval is on scale and when necessary conditions obtain, e.g., computer ready to accept data, and (b) the VTID circuitry. The latter consists of start and stop circulating loops and an inhibit circuit. An initial start pulse sets the upper loop into oscillation with a period determined by gate delays and by the RC time constant of the flip-flop utilized as a one-shot. This loop establishes T_1; the number of periods is recorded by a counter. The stop channel is constructed in an identical manner. The inhibit, or "kill coincidence" circuit accepts pulses from both, the start and the stop channel. The COIN FF changes states with each application of a start or stop pulse. However, the VETO one-shot is not triggered until the stop pulse has completely overlapped or is ahead of the start pulse, as shown in Figure 7. The duration of the veto pulses is longer than the period of either channel and this pulse is utilized to inhibit the circulating loops thus stopping the oscillators. The contents of two counters that record the number of recirculations are used to establish the time interval under measurement in accordance with Eq. (4).

This VTID has a variable resolution with a minimum of 16 ps/channel, and an integral linearity with a statistical confidence level of 27% to 81%, depending on channel width. Differential linearity was established to be within the statistical fluctuations of the measurement at 3500 counts/channel (±1.7%).

The intrinsic time resolution of this circuit (and of all VTID circuits), neglecting the problems associated with input pulse timing, may be expressed as $t_{resol} = \alpha + \beta\sqrt{n}$. α is the time jitter contributed by the input (start and stop) circuits and by the resolution of the inhibit circuit. The second term $\beta\sqrt{n}$, arises, from the phase noise in each oscillator; therefore, the uncertainty of the occurrence of the nth pulse (at coincidence) should be proportional to $\sqrt{n}$. This has been verified experimentally for the circuit of Figure 6 yielding $\alpha = 9.4$ ps and $\beta = 13.7$ ps. In practice the limitation on resolution are predominantly determined by the detector rather than the measuring circuitry. It has been shown (Ba 71) that for an intrinsic resolution that is half the detector resolution the total system's resolution is degraded by less than 12% due to circuitry.

The dynamic range of vernier measurements described earlier in this section cannot exceed the time expansion factor k. However, when $\tau > T_1$ the time expansion factor may be increased considerably through accumulation of several coincidences between the 2 clock phases. As shown in Figure 8 an up-down counter increments during the interval τ to record an integer number of T_1 periods. At $t = \tau$ the stop channel oscillator is activated having a period $T_2 < T_1$. Phase coincidences between the two oscillators are utilized to decrement the same counter. An output is obtained at time $k\tau$ when the counter has reached 0 state again, as shown in the last line of the figure.

Denoting by n_0 the number of integer up counts such that $n_0 T_1 \leq \tau$ and N_c the number of phase coincidences between the two oscillators, we deduce from Figure 8 the

total number of counts, N,

$$N = n_1 + N_1 N_c = n_2 + N_2 N_c \quad , \tag{5}$$

where the symbols of Eq. (5) are defined in the figure. Further, since $n_0 = n_1 - n_2$ and $N_1 T_1 = N_2 T_2$ it follows that

$$n_0 = N_c (N_2 - N_1) = N_c \quad , \tag{6}$$

since $N_2 - N_1 = 1$.

4. TIME OVERLAP PRINCIPLE

This time-to-amplitude converter evolved from coincidence circuits; its output amplitude is proportional to the time overlap of two pulses. As illustrated in Figure 9a input 1 precedes in time input 2 and the output amplitude is proportional to $T_1 - \tau$; hence T_1 must be well defined. Similarly should input 2 arrive first the output amplitude will be proportional to $T_2 - \tau$ (see Figure 9b). This sequence-dependent function is shown in Figure 10 for $T_1 = T_2 = T$. The deviation from linearity around $\tau = \pm T$ and $\tau = 0$ as shown by the full line is due to finite transition times of the input pulses. A supervisory circuit commonly precedes the converter to ensure that only those events are accepted which have the required input sequence; otherwise random coincidences are obtained.

Most of the TAC's designed around the time overlap principle yield an output only if the input pulses are separated by a time interval that is smaller than their duration. Unlike a start-stop TAC (see Section 5) no output is generated when only one input is applied to the circuit and the deadtime of the measurements is thus low.

One type of overlap TAC is shown in Figure 11. Initially Q_1 and Q_2 share equally a constant current I. A single input cuts off the respective transistor and I is carried by the other transistor of the differential pair resulting in a small voltage change at the common emitter point A, insufficient to bring Q_4 into conduction. During overlap of inputs 1 and 2 the voltage drop at A is sufficient to turn on Q_4 while Q_1 and Q_2 become back biased. C is thus charged via the constant current I and reaches a potential $I/C\ (T - \tau)$, where τ is the separation in time between the two input pulses. When one or both the input signals are removed, Q_4 stops conducting and the output waveform is determined by the time constant RC. Resolution of the circuit is better than 100 ps and the stability among other factors depends on the constant current source I. The pulse width is too narrow to be applied directly to pulse-height analyzers or for analog-to-digital converters, and further integration and voltage amplification are required.

In the circuit of Figure 11 $V_{out}(\tau) = V_{out}(-\tau)$ causing ambiguous results and doubling of coincidence rates. The single-valued overlap TAC of Figure 12a (We 65) overcomes this problem. R_L determines the operating points of the tunnel diode in the following four states as shown in Figure 12b: (a) Quiescent, with I_B (= bias current) determining point 1, (b) point 2 determined when a stop pulse only has been applied, (c) point 3 resulting from the coincidence of the stop and start pulses, and (d) point 4 when the start pulse has been removed. The circuit returns to its quiescent state when both input pulses have been removed. Waveforms are shown in Figure 12c. The output is derived at time $T_2 + t_d - (T_1 + t_d) = T_2 - T_1$ which is the time interval under measurement. The intrinsic resolution of the circuit is <40 ps with a temperature coefficient of 20 ps/°C.* It exhibits a very good integral linearity and has a differential linearity of 4% in its useful operating range of 10 ns. The circuit is, however, sensitive to high single rates since a single pulse moves the operating point from point 1 to point 2 resulting in a small voltage output. This single output is integrated and causes an offset error as shown in the lowest line of Figure 12c.

The integrator may include a bootstrap circuit to increase the open loop low frequency gain and thus generate a slow decay time constant that would allow sufficient time for digitizing. When an ADC is incorporated in the time measurement apparatus one should add a discharge circuit to reduce the integrator output to zero when the conversion to digital form has been completed; a higher conversion rate (time-to-digital) is thus obtained.

5. START-STOP PRINCIPLE

There are more instruments designed around this principle than any other time-interval measurement method and several references may be found in the bibliographical section. In this type of time-interval measurement a capacitor commences charging linearly at the arrival of a start pulse at T_1. The charging stops when a subsequent stop pulse is applied at T_2. The output voltage is thus linearly proportional to the time difference $T_2 - T_1 = \Delta T$. Depending on the subsequent circuitry the resultant signal may be shaped to match the input requirements of a pulse-height analyzer. Alternatively, the capacitor may be discharged linearly to its initial state while a gated oscillator is activated for the duration of the discharge allowing a counter to accumulate the number of counts recorded during the discharge period. Intrinsic time resolutions as low as 5 ps have been achieved (Br 65). Thus the contribution of this circuit to any degradation of the overall system's resolution is usually negligible.

A start pulse unaccompanied by a subsequent stop pulse produces an overflow charge on the capacitor (a voltage greater than the instrument can process linearly) with an attendant loss of utilization of time for conversion of valid events. This deadtime may be easily removed by use of a supervisory circuit that does not allow commencement of capacitor charging until the presence of a stop pulse within the time window, i.e., within the maximum time range has been ascertained. Such a system is then referred to as "start-ready-stop" (SRS). In SRS systems the duration of the start and stop pulses do not have to be well defined (unlike in time overlap circuits) and the time interval to be measured may thus exceed their duration.

Depending on the design details a circuit without supervisory logic may be symmetrical with respect to the start and stop pulses resulting in an even (symmetric) function $V(t) = V(-t)$ as shown in Figure 13.

A time-to-amplitude converter, TAC, operating on the start-ready-stop principle is shown in the block diagram of Figure 14 (Ta 72). As can be seen in the accompanying time diagram of Figure 15 the start and stop pulses are first shaped and the start pulse is delayed ① by a time interval not exceeding the time window ③. Thus a start channel can be activated only if the stop channel has generated a time window to allow the start pulse progressing past the time coincidence circuit ④. The start channel can, therefore, accept high data rates without causing any conversion deadtime losses for non-valid events in which no stop pulse has been applied to the system. This high data rate in one channel is typical of many nuclear measurements including experiments with accelerators.

The output from the time coincidence circuit ④ triggers a start single shot ⑤ which starts the linear charging of a range-selected capacitor shown in Figure 16. The same start single-shot pulse inhibits gate ⑨ to prevent further

*This temperature coefficient effect which is rather large in comparison with the intrinsic resolution can be reduced considerably by use of stabilization techniques discussed in Section 8.

stop pulses from reaching the stop channel circuitry. The trailing edge of the time window is differentiated and triggers the stop single-shot ⑥ provided the start channel has been previously activated.

The outputs from the start and stop single-shots are applied to the TAC of Figure 16 that operates as follows: in the quiescent state Q_{10}, Q_{12}, Q_{15} and Q_{17} are conducting and the charging capacitor, selected by SW1 according to the desired time-interval range to be measured, is discharged. Q_{14} and its associated components constitute a stabilized current source that in the quiescent state is steered via Q_{12} and Q_{17} to ground. When the start pulse turns off Q_{17} the range-selected capacitor is charged linearly by the constant current source. On application of a stop pulse this charging current is steered to ground via Q_{13} and in this state the charged capacitor sees a high impedance composed of the open collectors of Q_{12} and Q_{17} and the high input impedance of the FET gate of Q_{18}. The circuit remains in this state until the start pulse has been removed. The duration of the flat top of the output signal (see ⑦ of Figure 15) is thus determined by the start single-shot and may be chosen to match the requirements of a PHA. Alternatively the termination of the start gate may be initiated through a signal signifying that the analog-to-digital conversion has been completed.

The supervisory circuit of Figure 14 was constructed from MECL II logic that was preceded by discrete circuitry for pulse amplitude standardization and level shifting.

When a spectrum random in time is applied to a TAC the number of pulses recorded in each channel should be equal within the statistics of the events per channel. If such a flat distribution is not obtained differential non-linearities are indicated. The origin of these non-linearities is due to fast switching transients and ground loops that couple the start and stop channels. Fast switching elements such as tunnel diodes, snap diodes, and grounded-base transistors are especially prone to this noise and should be carefully shielded and decoupled. In contrast, emitter-coupled non-saturated circuits are well suited for TAC design since little net effect is observed on the power supply and ground lines due to their current switching symmetry. Differential non-linearities for various operating conditions of the previously described circuit are shown in Figures 17a, b, and c. These were obtained using a ^{60}Co source to generate random time events that were applied to the stop channel. A variable frequency pulser was utilized to generate pulses for the start channel in testing the rate dependence of the system.

Note that in Figure 17b only half the spectrum is available when the input rate to the start channel corresponds to half the period of the time window. This phenomenon is caused by early triggering of the start single shot which inhibits gate ⑨ in Figure 14 and thus does not allow for conditions in which $T_{stop} - T_{start} < 100$ ns; i.e., since the start channel responds to the first valid time coincidence ④ a unity probability exists for the start channel to be triggered in the first 100 ns resulting in the spectrum blanking as shown in Figure 17b for a 10 MHz rate and a time window of 200 ns. Figure 17d shows the time resolution of 105 ps/channel, fwhm, for peaks A and B obtained with a pulser input to both channels with relative delay. A random time spectrum was also superposed to define the time range. Peak C was obtained after the amplifier gain was increased to obtain an expanded time spectrum. A resolution of <60 ps/channel, fwhm, is indicated.

A summary of methods of time-interval measurements is shown in the table.

METHODS OF TIME-INTERVAL MEASUREMENTS IN THE SUBNANOSECOND REGION

	Resolving Time	Dynamic Range	Long Term Stability	Linearity	
				Integral	Differential
1. Counter	≥ 500 ps	No Limit in Principle	Very Good	Very Good	Very Good
2. Counter + Coincidence	≥ 200 ps	No Limit in Principle	Very Good	Very Good	Good(2)
3. Vernier with Single Coincidence, $\tau < T_1$	≥ 15 ps	≤ 500(1)	Very Good to Good	Very Good	Good
4. Vernier with Multiple Coincidences, $\tau > T_1$	≥ 200 ps	$10^3 - 10^4$ (1)	Very Good	Very Good	Good
5. Overlap Coincidence	≳ 5 ps	500(1)	Poor(3)	Very Good(4)	Good(4)
6. Start-Stop	≳ 5 ps	500(1)	Poor(3)	Very Good(4)	Good(4)
7. Microwave	< 1 ps (5)	100	Poor to Good (5)	Good	Poor to Good

(1) Practical limit.
(2) Can be improved using auxiliary derandomizing circuit.
(3) Can be improved considerably by feedback stabilization.
(4) Except at both ends of time range.
(5) Depends on frequency used.

2285A23

6. PICOSECOND TIME-INTERVAL MEASUREMENTS USING MICROWAVE TECHNIQUES (Gu 73)

This method has the highest resolution, a moderate stability and its use is limited to situations in which the time-interval to be measured shows an intrinsic RF structure or where RF modulation may be imposed. Consider acceleration of charged particles such as protons, electrons, etc., by use of radio frequency fields; the phase of the RF field is matched to the velocity of the particles to ensure an accelerating field vector on their passage through the RF accelerating structures (cavities). The net effect results in "bunching" of the charged particles in a narrow phase space. Thus, for example, in the Stanford 2-mile linear accelerator which operates at 2856 MHz the separation between the bunches is 350 ps and each bunch occupies an RF phase of 5 degrees corresponding to a 5 ps time spread in every 350 ps interval. It follows that charged particles produced in interactions or decays originate with the same time structure. Since the time resolution of the best photomultipliers is about 2 orders of magnitude worse, some other technique has to be used to take full advantage of the narrow time spread of the originating particles. An RF separator operating at the same frequency as the accelerator microwave structure has the requisite characteristics: a charged particle traversing such a separator will be deflected by a distance that is proportional to the relative RF phase angle that it experiences during its traversal. Time-interval measurements may be made with respect to reference particles that enter the separator at an RF phase corresponding to null deflection. Thus a time-interval measurement has now been changed to a position measurement which can be effected with very high spatial resolution using multiwire proportional chambers. A sub-picosecond time-interval resolution was reported using this method (Gu 73).

7. TIME SCALE CALIBRATION

One method of time scale calibration mentioned earlier utilizes a radioactive (e.g., ^{60}Co) source to produce pulses at random time intervals. These are applied to the stop channel of a time analyzer while the output of a pulse generator of suitable frequency is applied to the start channel. The random time intervals thus generated are displayed on a pulse-height analyzer display and should produce the same number of counts in each time channel within the statistical fluctuations of the recorded counts per channel. The variations of pulse amplitude generated by the radioactive source introduce a limit to the accuracy of these measurements because of the inherent time walk for pulses whose amplitude is in the vicinity of the threshold of the discriminator-shaper circuit that has to be used in the stop channel. The method may be improved through pulse amplitude selection utilizing a second discriminator which is set at a higher threshold than the stop channel discriminator to ensure via coincidence gating that all pulses used for calibration are well above an amplitude where time walk is of no significance. The calibration yields information on differential linearity, from which integral linearity may be easily deduced by observing the slope of number of counts versus PHA channel.

An absolute calibration of channel width is obtained by superposing two peaks on the random time spectrum using a resistively split pulse from a fast pulse generator with a variable delay in one channel. A General Radio Trombone delay line type 874-LTL with a Bishop Instrument Trombone Setter model 011-001 yielded delay measurements to an accuracy of ±5 ps in the range of 0 to 32 ns (Ta 69).

A resolution of < 40 ps/channel, fwhm, was obtained (We 65) when both channels in a start-stop TAC were driven from a single photomultiplier using amplitude selected pulses. A variable delay was inserted in one channel with an adjustment resolution of 0.3 mm corresponding to 1 ps.

In a similar method (Ta 68) a helical air insulated delay drum was used which was driven by a small synchronous motor. Output pulses from a constant frequency pulse generator were fed into two transmission lines one of which included the helical delay. Differential linearity was measured by driving the delay drum over the desired delay region and accumulating the outcoming time spectrum. The delay factor of the drum used was 6.45 ps/s and a pulse frequency of 1 kHz. A differential linearity of ±5% over a useful operating region was found and an integral linearity of ±0.2% in the same region.

The inherent small time jitter of a sampling sweep in a sampling type scope provided a simple method for time calibration down to the ps region (Ch 70). The method used the delayed sampling pulses that were obtained with help of two auxiliary signal pickoff circuits that are attached to a commercially available sampling time base.

As seen in Figure 18 every input event starts a fast ramp, these ramps being triggered at successively higher thresholds. Timing pulses are generated at the instants of starting a ramp as well as at the threshold (sampling) levels. Thus each event produces a pulse pair with a delay equal to the integral multiple of a time T as shown in the last line of Figure 18. T is variable since it can be set by the scope time-scale setting. For example the minimum setting of a Tektronix 3T77 sampling sweep unit is 200 ps. Thus a minimum T of 2 ps may be obtained at a setting of 200 ps/100 sampling points. The pulse pairs thus generated are applied as start and stop signals, respectively, to a time-to-pulse-height converter as shown in Figure 19. A signal source is required to trigger the ramp but any signal source is suitable since the time interval between pulse pairs is relatively independent of the input pulse distribution (see interval 3T, third line of Figure 18). The problem of inherent integral non-linearily of the fast ramp may be overcome by use of only the linear portion of the ramp since the number of calibration peaks is much smaller than the number of pulse pairs generated at each sweep.

Calibration results are shown in Figure 20. The upper spectrum was obtained with random input pulses while the lower two spectra were obtained with periodic input pulses. The time scale change was effected by changing the setting of the scope. For example, with a Tektronix 3T77 sweep unit calibration peaks with intervals of up to 1 μs are achievable.

A random-time, random-amplitude generator is described by Dechamps et al. (De 70) where it is shown that with rather simple transfer functions such as RC integration or differentiation a transformation of a Poisson distribution into a uniform distribution may be achieved. To generate random-time pulses with a Poisson distribution the noise of an operational amplifier, type μA 702 was used.

8. STABILIZATION OF TIME-INTERVAL MEASUREMENTS

In the previous sections we have discussed time-interval measurements with a resolution < 10 ps. This quantity is about two orders of magnitude lower than the transition times of the semiconductors used in the measurements. Such measurements are quite often of long duration to ensure better statistical results especially when the cross sections of the events to be investigated are very small.

Time-interval measuring systems are subject to noise and to slow drifts of component values, propagation delay times, and temperature dependent parameters. The noise problem is usually reduced through careful shielding of those components exhibiting the fastest transistion times, to minimize their radiation effects. Also, these components are well decoupled from common power supply lines and a low impedance ground bus is mandatory. Special care must

be exercised to prevent coupling of signals between the input channels of a TAC such as the start and stop terminals. Additionally, if noise can be reduced to be predominantly of a random nature its contribution to the spectrum width can be reduced through better statistics which improves the randomly generated broadening of a peak by a factor of $N^{-1/2}$ where N is the number of accumulated counts.

Systematic changes, however, such as temperature dependent drift, cannot be reduced through statistical means. Since they are slow in nature, a feedback system is best suited to remove their contributions to errors. A block diagram of a feedback loop is shown in Figure 21. In normal operation the system consists of the circuits indicated by lightly outlined rectangles. The heavily outlined rectangles constitute the components required for the stabilizing feedback loop. A time reference generator produces fast rising pulses at regular intervals, e.g., 1 pps. The pulses are split into two channels and attenuated to absorb any reflections. When the switches are in the test mode the two pulses are applied to the TAC or TDC, one pulse undergoing a well defined and stable delay. The shaper and trigger circuitry and the supervisory logic are included in the calibration path since the loop should correct for as many drift sources as possible. In the test mode an output of a fixed predetermined amplitude (if TAC) or number of counts (if TDC) is expected for a given setting of the precision delay in the stabilizing loop. This output is held as an analog quantity V_{REF} or as a number, N_{REF} which is compared with the TAC or TDC output on every calibration cycle of the stabilizing loop. The difference, $\pm \Delta V$ or $\pm \Delta N$ is applied to an error correction circuit and thence to the TAC or TDC to bring the calibration peak into the desired channel (amplitude or binary number).

A digitally stabilized timing system is described in reference (Ka 72). Upper and lower reference channels are first set up and a correction, negative or positive, is applied to the TAC. A line broadening of the spectrum is generated as a result of statistical fluctuations in the reference channels. This source of broadening has been reduced (Ka 72) by applying the error voltage to an integration circuit with a time constant much greater than the fluctuation period, yet shorter than the time constants of the system's drifts. The integrated error is then applied to the ADC circuitry of the time analyzer.

Note that in Figure 21 the time reference is obtained from a generator. Since detectors are also subject to transit time variations, a more appropriate point of pickoff would be at the outputs from the photomultipliers. The drifts in the photomultipliers are principally due to high-voltage instability and hence appear as a common-mode, second-order effect. A stabilizing loop may be effected with analog, digital and mixed (analog-digital) techniques. Any effective loop should include the following capabilities: (a) change in conversion gain of the TAC or TDC, (b) shift of intercept(s), (c) negligible influence due to stabilization on the width of the spectrum, and (d) negligible random coincidences between the reference and event measurements.

The bibliographical section lists a number of references describing stabilization systems. Most of these pertain to stabilization of pulse amplitude spectra. However, many of the techniques referenced may be applied, with suitable modifications, to stabilization of time-interval spectra.

9. APPLICATIONS AND CORRECTIONS FOR TIME WALK

Time-interval measurements are widely used in nuclear structure and in particle physics experiments for determination of lifetimes of excited states, time-of-flight measurements, identification of particles, etc. For example, the mass resolution in a heavy-ion spectrometer can be obtained by the time-of-flight method with much greater accuracy than using a dE/dX-E method. Assume that $\Delta E/E$ is the intrinsic energy resolution of a detector, $\Delta t/t$ the time resolution of the time measuring instrument, and $\Delta s/s$ the distance (path-of-flight) resolution. It can be easily shown (Ge 71) that the mass resolution $\Delta m/m$ is obtained from

$$(\Delta m/m)^2 = (\Delta E/E)^2 + (2\,\Delta t/t)^2 + (2\,\Delta s/s)^2 \qquad (7)$$

With $\Delta E/E \approx 0.5\%$ for heavy ions in a solid state detector $\Delta t/t$ should ideally be of the same order of magnitude to optimize Eq. (7). This would require either a long flight path which has the disadvantage of reducing the solid angle, or a better time-interval measurement. The mass resolution as a function of energy per nucleon is shown in Figure 22a with variable parameters as shown in Figure 22b (Ge 71).

In time-of-flight measurements of minimum ionizing particles the problem of time walk arises from signals near the threshold of the discriminator-shaper circuits. This is illustrated in Figure 23 (Ba 72) in which the inputs to a discriminator as a function of time are shown for three different pulse sizes. Since trigger circuits are usually charge sensitive, the discriminator fires at times t_1, t_2, and t_3, somewhat below the discrimination level that is shown by the dashed line. The resultant time spectra are shown on the right-hand side of the figure. K in the abcissa is an arbitrary constant.

Three methods are currently employed to minimize the amplitude dependent time walk for improved time definition in short time-interval measurements. In method 1 the objective is achieved through utilization of leading edge triggering, zero crossing circuits or "constant fraction" triggering.

The effectiveness of this method depends primarily on the pulse characteristics and the various options available in method 1 will thus be chosen accordingly. In any case, this method does not yield time definitions that are nearly as good as in the two methods described below.

In method 2 the pulses are normally applied to a TAC and simultaneously they are operated upon in parallel channels using non-linear compensation functions. The circuit operates on the input pulses V_{in} of a TAC to generate compensating output voltages $\Delta V_{out} = f(V_{in})$. The outputs from the compensators (one in the start and the other in the stop channel) are then linearly mixed with the TAC output to attain a well compensated time-interval measurement.

In the third method auxiliary ADC's are used to measure the amplitudes of each start and stop pulse. With a known time walk dependence of a given discriminator the raw output from the time-interval measuring device can be corrected in the data-logging computer.

The last two methods are discussed below in greater detail. They are similar in that they utilize auxiliary ADC's to determine the amplitudes of the signals that are applied to the time-interval measuring apparatus. A block diagram of method 2 is shown in Figure 24 (Ba 72); start and stop pulses are applied to amplitude sensitive non-linear compensation circuits and each pulse thus corrected for time walk is mixed with the TAC output before being applied to the time digitizer. The components constituting the compensation are shown in dashed lines.

Uncompensated walk curves are not straight lines and thus linearly dependent amplitude corrections take care of first order effects only. Higher order effects may be included in the compensation by use of non-linear functions of pulse amplitudes. A simple non-linear compensation function is shown in Figure 25 and consists of two variable resistors and a diode. The resistors and the amplifier following it are adjusted for minimum time walk in the pulse height of interest. Pulses that are not in that range are rejected on the basis of ADC measurements. This system, sometimes referred to as the "analog post-clock pulse-height

compensator" is simple to implement and has improved the time walk by a factor of 20 (down to 3±3 ps) over a limited energy range (Ba 72).

Since the uncompensated time walk is very nearly a logarithmic function, compensation over a broad energy range should be possible using active circuits.

The third method in minimizing the time walk problem is of a more general nature. The typical response of two discriminator circuits is shown in Figure 26 (Ba 73). When the amplitude applied to the discriminator is known, corrections may be derived from the known or previously calibrated time-walk versus input-amplitude relationship. The technique is especially adapted to computer controlled data-acquisition systems since errors due to time walk can be corrected by the data logging computer before the time spectrum is established. This technique, for example, has been extensively used in K^0 decay studies (En 71, Ak 72, Pi 72) utilizing a circuit that is capable of measuring amplitude as well as time intervals with a resolution < 100 ps in time and < 0.5% in amplitude (Po 69, Po 71).

ACKNOWLEDGEMENTS

Thanks are due to Ray Larsen, Arpad Barna, Bill Jackson, Fred Kirsten and Richard Spitzer for fruitful discussions. I am indebted to Dave Hitlin and Steve Shapiro for reading the manuscript and for their constructive comments.

BIBLIOGRAPHY FOR SUB-NANOSECOND TIME-INTERVAL MEASUREMENTS

Reviews

Bo 62 M. Bonitz, NIM 22 (1963) 238.
Me 68 W. Meiling and F. Story, Nanosecond Pulse Techniques, Gordon and Breach Sci. Publ., 1968, Section 3.4.
Og 68 A. Ogata, S. J. Tao and J. H. Green, NIM 60 (1968) 141.
Sc 63 A. Schwarzschild, NIM 21 (1963) 1.
Zu 71 R. Van Zurk, Proc. Int'l. Symp. Nucl. Electronics, Warsaw, September 1971.

Time-to-Digital Converters

Lo 64 I. De Lotto, E. Gatti and F. Vaghi in Proc. Conf. Automatic Acquisition and Reduction of Nuclear Data, EANDC, Karlsruhe, 1964, 291.
Me 66 H. Meyer, NIM 40 (1966) 149.
Po 69 F. Požar, NIM 74 (1969) 315.

Vernier Principle

Av 70 J. Aveynier and R. Van Zurk, NIM 78 (1970) 161.
Ba 57 R. G. Baron, Proc. IRE 45 (1957) 21.
Ba 71 R. D. Barton and M. E. King, NIM 97 (1971) 359.
Co 58 C. Cottini, E. Gatti and F. Vaghi, Proc. Conf. Nucl. Electronics, Paris, 1958.
Ki 66 P. J. Kindlemann and J. Sunderland, Rev. Sci. Instr. 37 (1966) 445.
Le 59 H. W. Lefevre and J. T. Russel, Rev. Sci. Instr. 30 (1959) 159.
Th 66 J. Thenard and G. Victor, NIM 40 (1966) 318.
Ve 66 W. H. Venable, Jr., Rev. Sci. Instr. 37 (1966) 1443.

Time Overlap and Start-Stop Principles

Bc 65 J. Bell, S. J. Tao and J. H. Green, NIM 35 (1965) 213.
Be 65a J. Bell, S. J. Tao and J. H. Green, NIM 36 (1965) 320.
Be 65b R. E. Bell in Alpha-Beta-and-Gamma-Ray Spectroscopy, Ed. K. Siegbahn, North-Holland Publ. Co., Amsterdam, 1965.
Bi 72 J. Bialkowski and M. Moszynski, NIM 105 (1972) 51.
Br 65 H. Brafman, NIM 34 (1965) 239.
Da 67 C. Dardini, G. Iaci, M. Lo Savio and R. Visentin, NIM 47 (1967) 233.
Dr 70 T. Droege, IEEE Trans. Nucl. Sci. NS-17 (1970) 445.
Le 71 LeCroy Research Systems, LRS 2226A (1971).
Og 69 A. Ogata and S. J. Tao, NIM 69 (1969) 344.
Ta 65 S. J. Tao, J. Bell and J. H. Green, NIM 35 (1965) 222.
Ta 68 A. Tamminen and P. Jauho, NIM 65 (1968) 132.
Ta 72 I. J. Taylor and T. H. Becker, NIM 99 (1972) 387.
We 65 H. Weisberg, NIM 32 (1965) 133.
Wi 63 D. L. Wieber, NIM 24 (1963) 269.

Picosecond Time Intervals

Gu 73 Z.G.T. Guiragossian et al., 1973 Particle Accelerator Conf., San Francisco, California, 1973; Report No. HEPL 705, Stanford University (1973).

Delay and Time Scale Calibration

Ba 68 C. A. Baker, C. J. Batty and L. E. Williams, NIM 59 (1968) 125.
Be 69 M. Bertolaccini and S. Cova, Proc. Ispra Nucl. Electronics Symp., May 1969, 119.
Ch 67 Z. H. Cho, L. Giedefeld and L. Eriksson, NIM 52 (1967) 120.
Ch 70 Z. H. Cho and C. Bohm, NIM 84 (1970) 327.
De 70 J. Dechamps, A. Hrisoho and B. Soucek, NIM 84 (1970) 253.
Jo 68 F. A. Johnson, NIM 59 (1968) 237.
La 68 A. Langsford and P. E. Dolley, NIM 59 (1968) 125.
Ta 69 H. E. Taylor, NIM 68 (1969) 160.

Spectrum Stabilization Methods

Ge 66 E. A. Gere and G. L. Miller, IEEE Trans. Nucl. Sci. NS-13, No. 3 (1966) 508.
Gr 70 J. Grinberg, B. Sabbah and M. Shuster, NIM 82 (1970) 278.
Ka 71 Y. Kawarasaki and T. Shoji, NIM 96 (1971) 347.
Ka 72 L. Karlsson, NIM 105 (1972) 349.
Le 70 F. R. Lenkszus and S. J. Rudnick, IEEE Trans. Nucl. Sci. NS-17, No. 1 (1970) 285.
Ma 69 M. Matoba and I. Kumabe, NIM 74 (1969) 70.
Na 65 M. Nakamura and L. La Pierre, NIM 32 (1965) 277.
Pa 66 A. Pakkanen and F. Stenman, NIM 44 (1966) 321.
Ro 69 L. B. Robinson and F. S. Goulding, NIM 75 (1969) 117.
Wi 66 D. Williams, G. F. Snelling and J. Pickup, NIM 39 (1966) 141.

Applications and Corrections for Time Walk

Ak 72 G. Akavia et al., Report No. SLAC-145, Stanford Linear Accelerator Center (1972).
Ba 72 R. D. Barton and M. E. King, NIM 100 (1972) 165.
Ba 73 A. Barna, "High Speed Pulse Instrumentation Techniques," Stanford Linear Accelerator Center (March 31, 1973).
En 71 J. Enstrom et al., Phys. Rev. C 4 (1971) 2629.
Fo 68 J. P. Fouan and J. P. Passerieux, NIM 62 (1963) 327.
Ge 71 C. K. Gelbke, K. D. Hildebrand and R. Bock, NIM 95 (1971) 397.
Pi 72 R. Piccioni et al., Phys. Rev. Lett. 29 (1972) 1412.
Po 69 D. Porat and K. Hense, NIM 67 (1969) 229.
Po 71 D. Porat and D. Ouimette, Report Nos. SLAC-TN-71-13, SLAC-TN-71-14, Stanford Linear Accelerator Center (June 1971).

DAN I. PORAT obtained his M.Sc. in Physics and Ph.D. in EE from the Manchester University, England. He was a Research Fellow at Harvard University (1959-62) and since 1962 has been on the staff of the Stanford Linear Accelerator Center, Stanford University. Dr. Porat specializes in nuclear instrumentation design including real time data-acquisition systems for scientific research. He is a Senior Member of the IEEE and has published 30 papers. He is co-author with Dr. A. Barna of Integrated Circuits in Digital Electronics (Wiley-Interscience, New York, 1973).

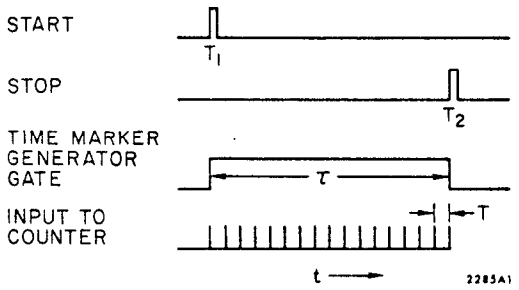

Figure 1. Time-to-digital converter; timing diagram.

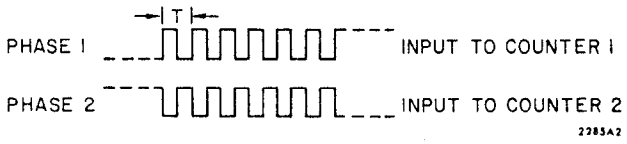

Figure 2. The resolution of a TDC is improved by a factor of 2 utilizing two oscillators that are synchronized to start on opposite phases. Two counters are required.

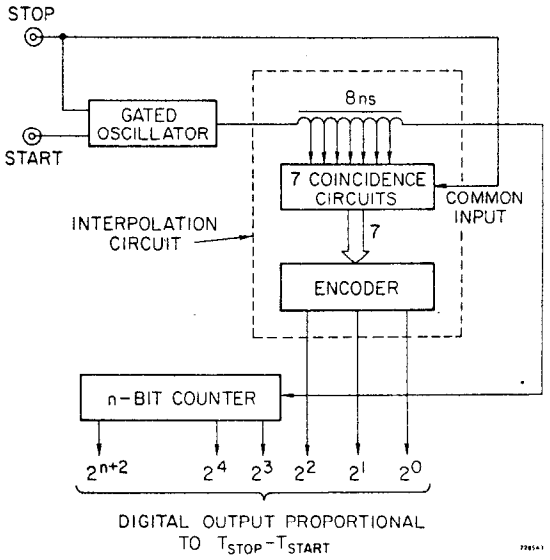

Figure 3. Time-to-digital converter with interpolation circuit to obtain 1 ns resolution using a 125 MHz clock.

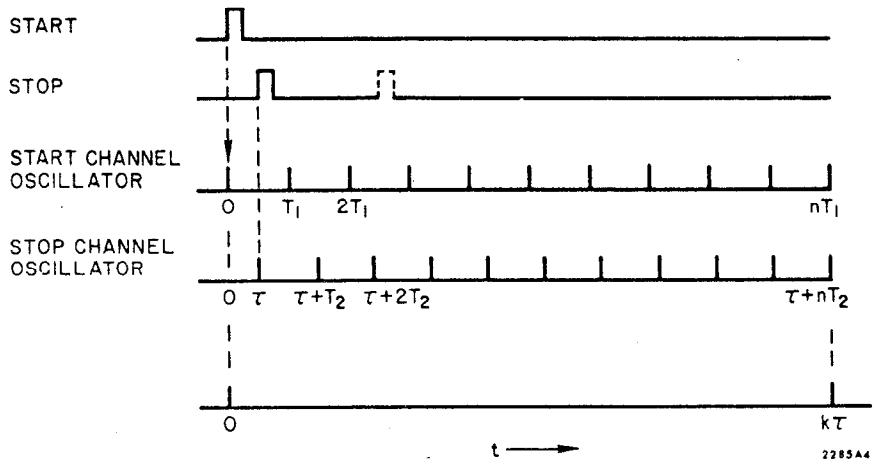

Figure 4. Time expansion using the vernier principle.

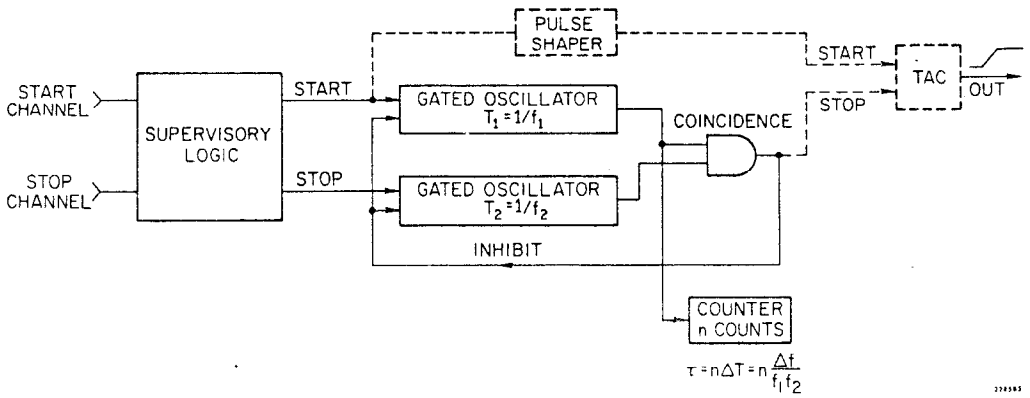

Figure 5. Vernier time-interval measurement circuit; block diagram.

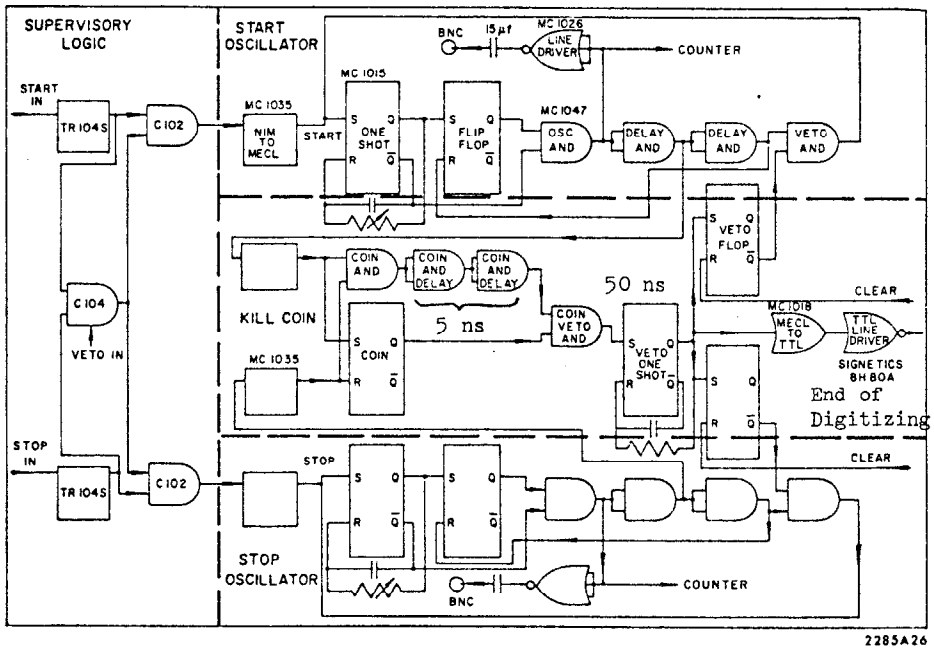

Figure 6. Vernier time-interval digitizer, VTID; schematic (Ba 71).

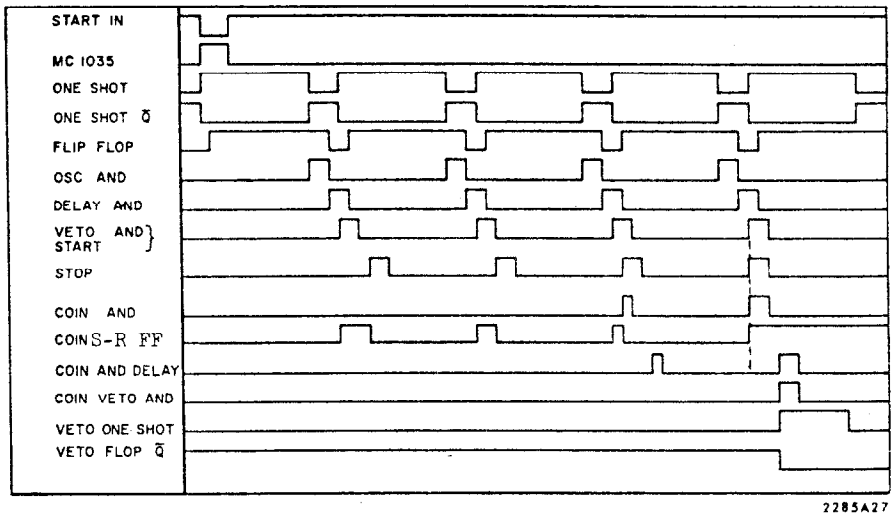

Figure 7. Timing diagram for the VTID shown in Figure 6 (Ba 71).

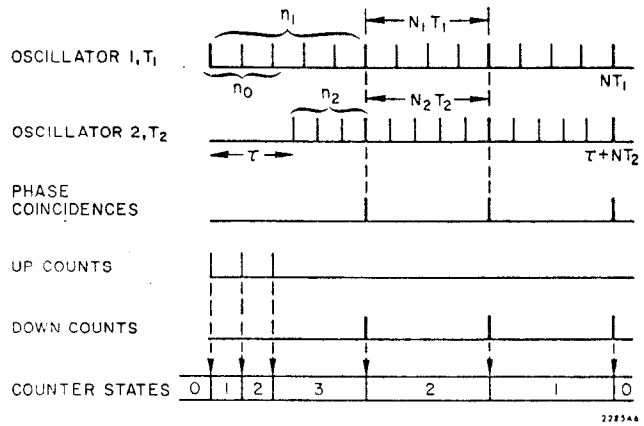

Figure 8. Vernier chronotron for $\tau > T_1$; timing diagram.

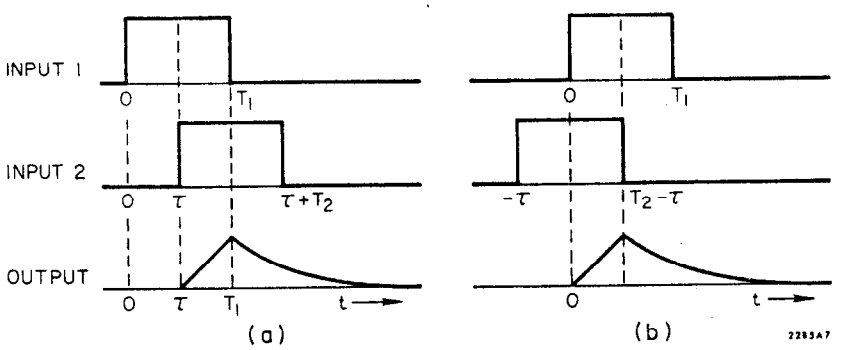

Figure 9. Time-to-amplitude converter, TAC, using the time-overlap principle; timing waveforms.

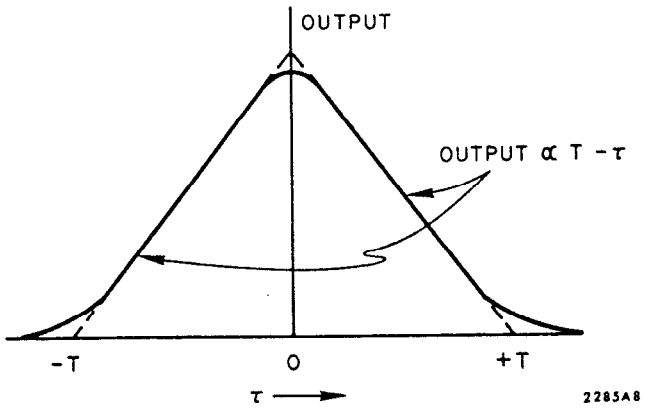

Figure 10. Output amplitude versus delay τ in a time-overlap TAC for $T_1=T_2=T$.

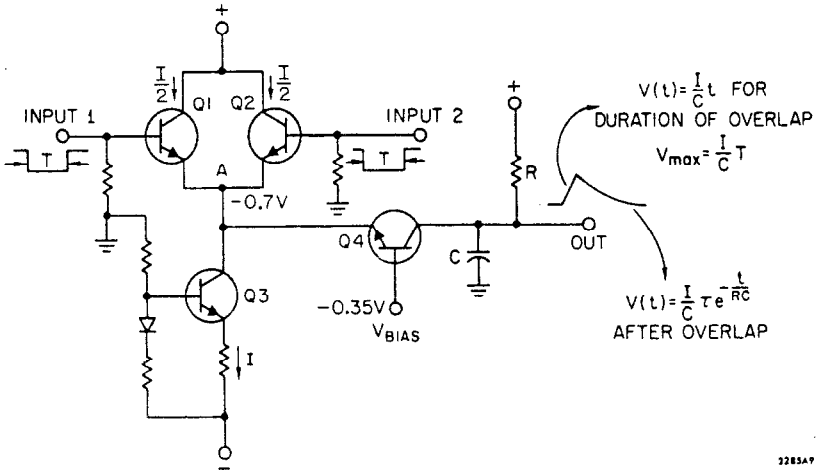

Figure 11. Schematic of a time-overlap TAC. Overlap duration is $T-\tau$ as shown in Figure 9.

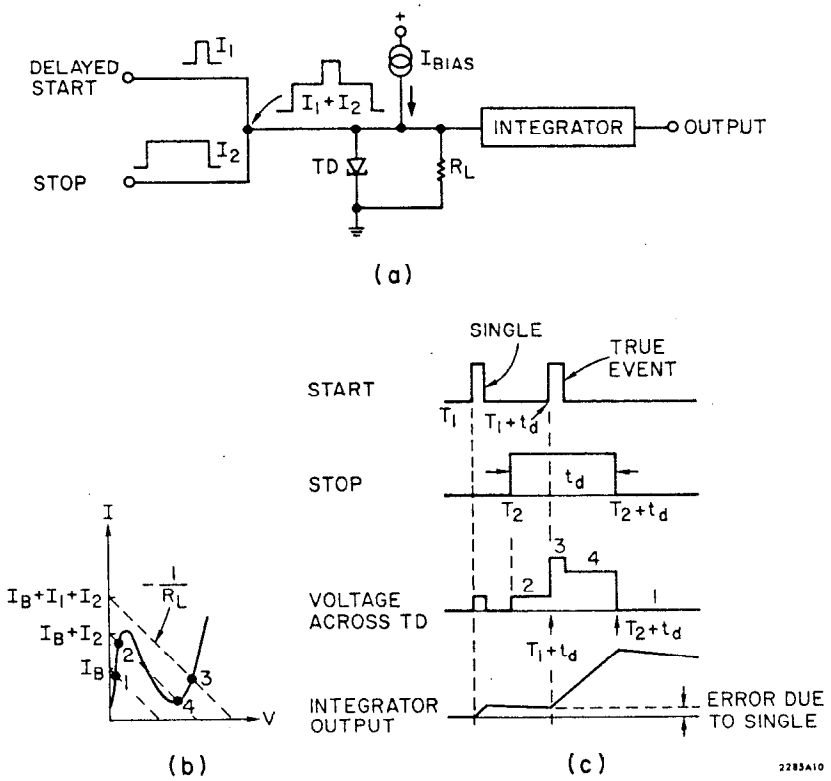

Figure 12. Time overlap TAC yielding a single-valued output (We 65): (a) Schematic (b) Operating points of the tunnel diode, TD. I_B = bias current, I_1, I_2 = currents from start and stop channels, respectively (c) Timing waveforms. The numbering on the waveform corresponds to the stable operating points of Figure 12b.

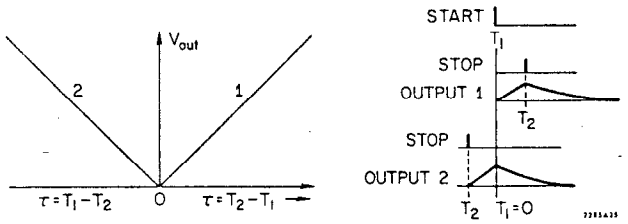

Figure 13. An even function, V(t) = V(-t) is obtained in a start-stop TAC when its circuit is symmetrical with respect to its two inputs.

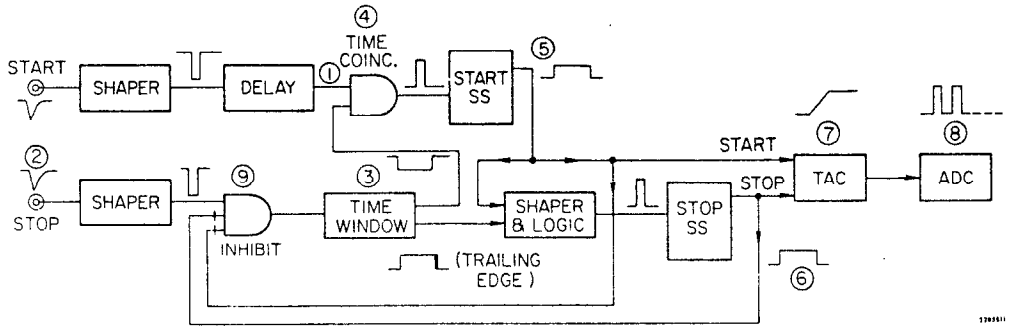

Figure 14. Block diagram of a start-ready-stop TAC (Ta 72). Circled numbers refer to timing diagram of Figure 15.

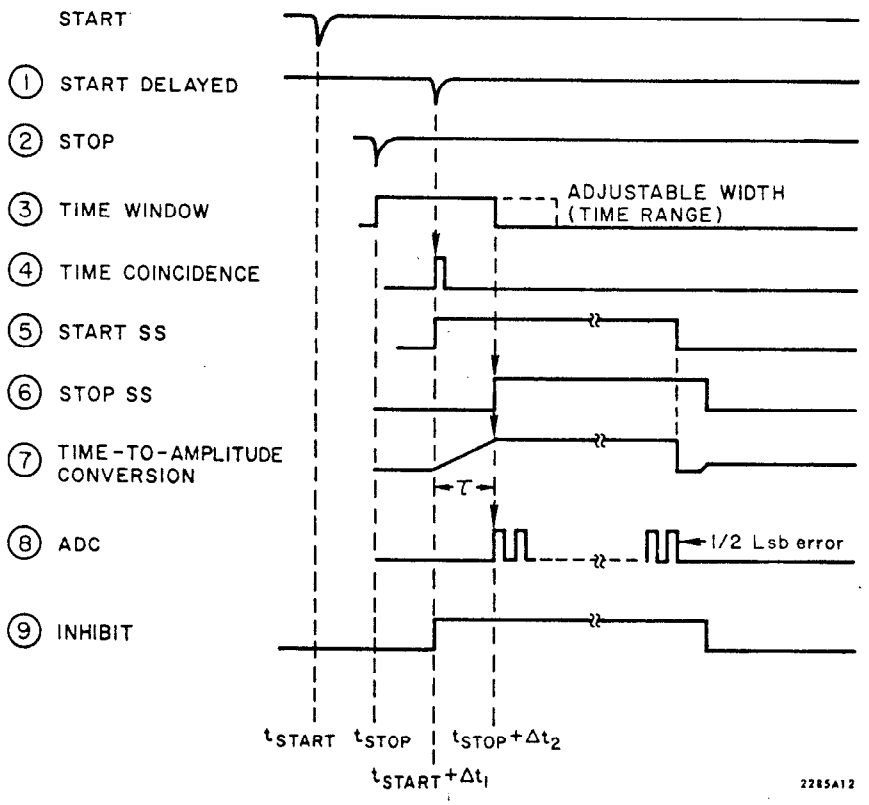

Figure 15. Timing diagram of the start-ready-stop TAC of Figure 14.

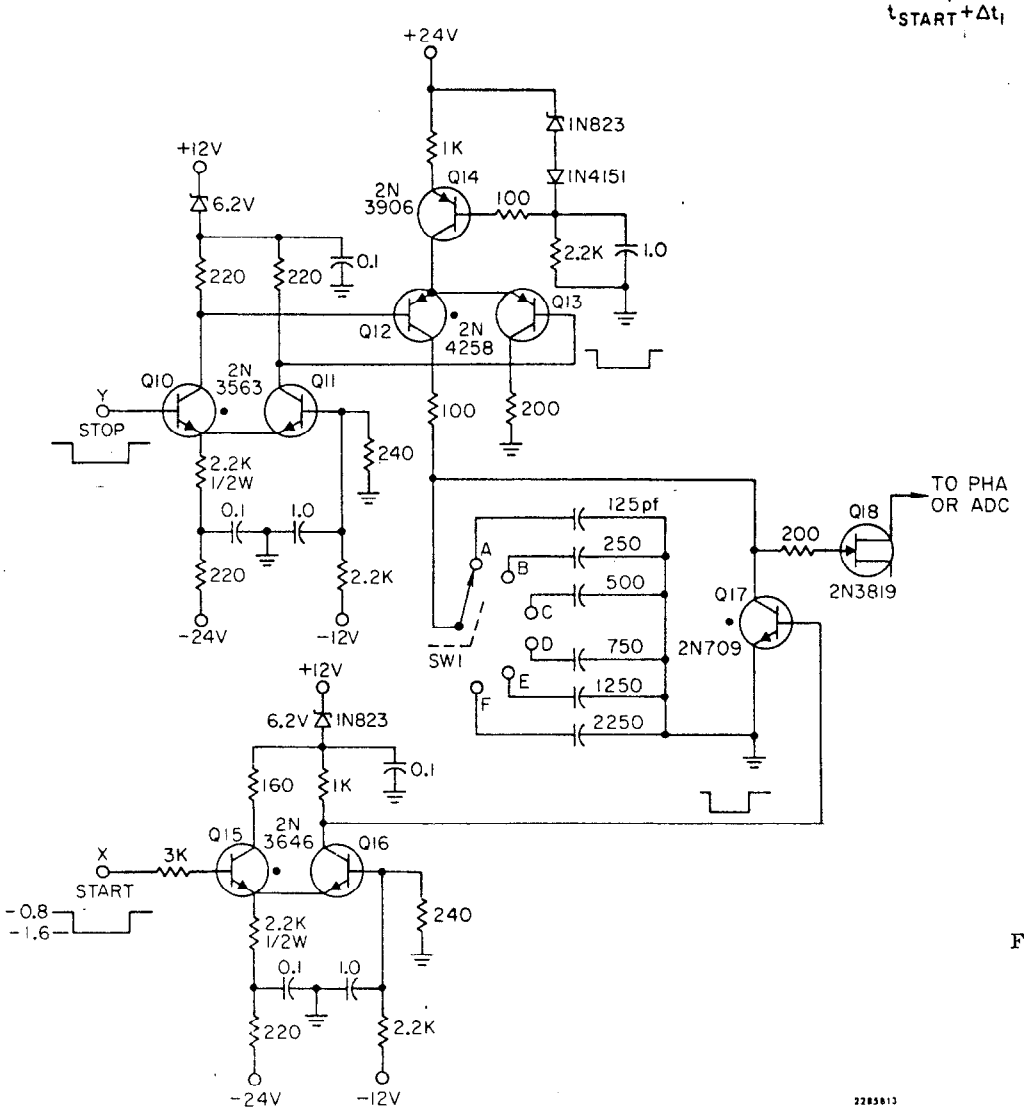

Figure 16. Analog section of the TAC of Figure 14; simplified schematic.

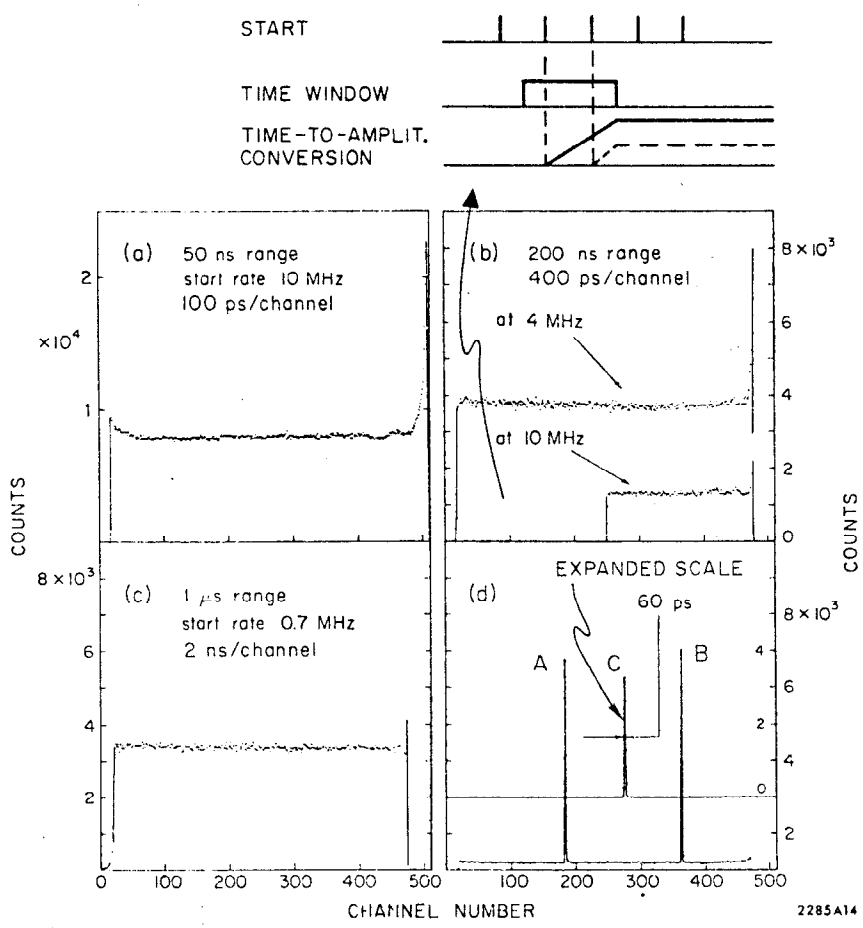

Figure 17. A series of random time spectra for some of the time ranges of the TAC of Figures 14 and 16. The pulse pair resolution is shown in Figure 17d and was obtained at ≈ 2 pps. The intrinsic resolution of 60 ps, see peak C, was obtained with an expanded scale.

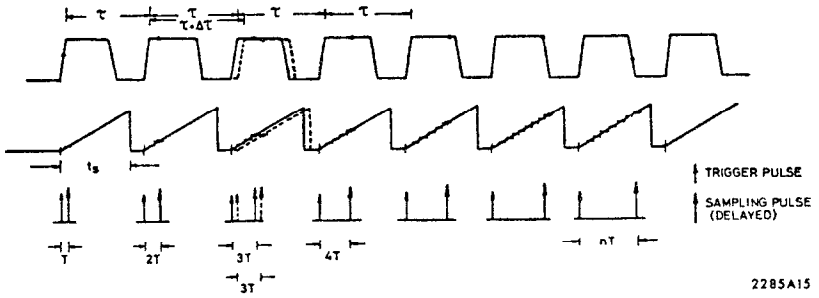

Figure 18. Principles of sampling scope operation. Upper line shows an input signal with a period τ. The middle line shows the fast ramps generated from the triggers at each positive transition of the input. The horizontal bars show the sampling points that are delayed by a time interval T for each successive input. The lower line shows time intervals T, 2T ... nT obtained via pickoff circuits. The dashed waveform demonstrates that the pulse pair interval is relatively independent of the input pulse distribution.

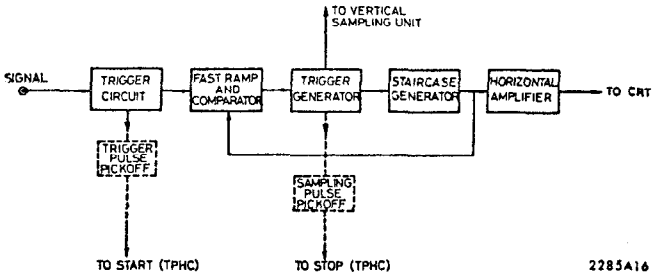

Figure 19. Simplified diagram of the sampling sweep unit (full lines) and additional trigger and sampling pickoff circuits (dashed lines), (Ch 70).

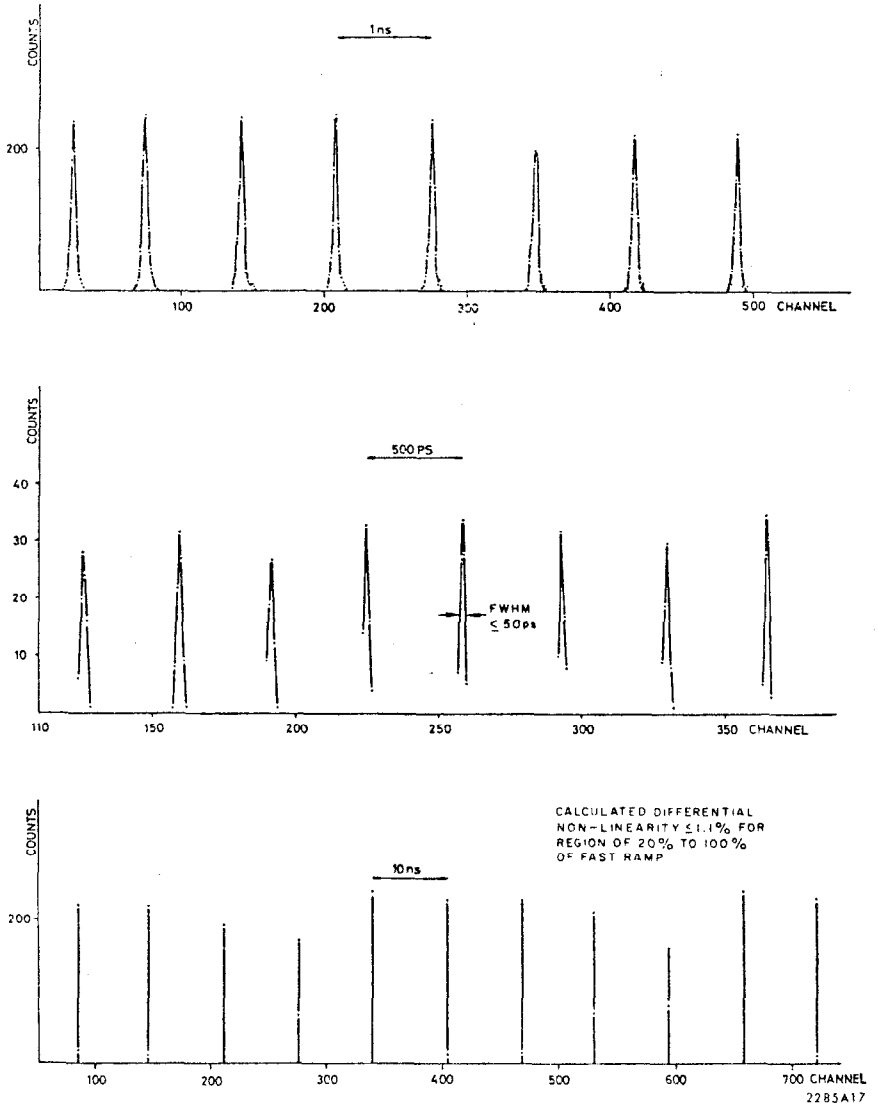

Figure 20. Calibration spectra using the circuit of Figure 19. (a) Random input pulses. (b) Periodic input signal; 15 ps/channel (c) Periodic input signal; 160 ps/channel.

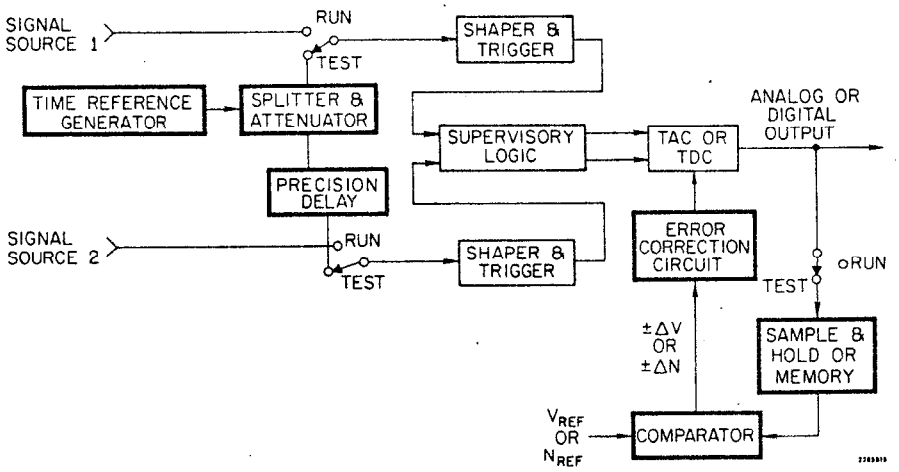

Figure 21. Block diagram of a stabilizing feedback loop for time-interval measurements.

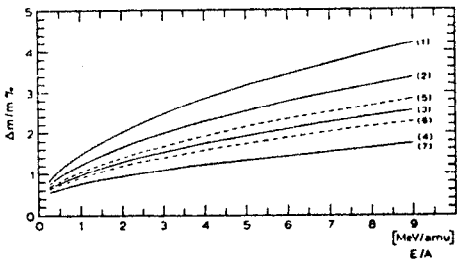

(a)

Parameters

Curve number	s (cm)	Δt (ps)
1	100	500
2	100	400
3	100	300
4	100	200
5	150	500
6	150	400
7	150	300

(b)

2285A28

Figure 22. (a) Mass resolution of a time-of-flight spectrometer (Ge 71).
Abcissa: Energy/atomic mass units (MeV/amu)
Ordinate: Mass resolution Δm/m, %.
(b) Parameters s and Δt for the curves of Figure 22a.

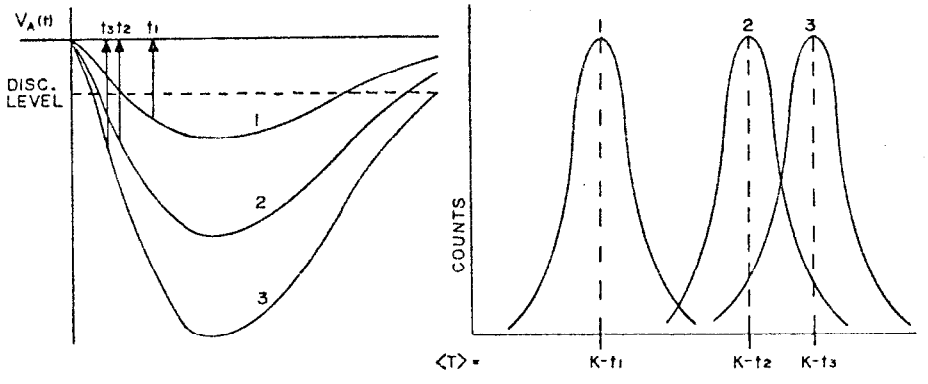

(a) (b)

2285A19

Figure 23. Time-walk due to three different input pulses applied to a discriminator with a fixed threshold. (a) t_1, t_2, and t_3 are the times at which the discriminator fires (b) Shift in time spectra. K is an arbitrary constant.

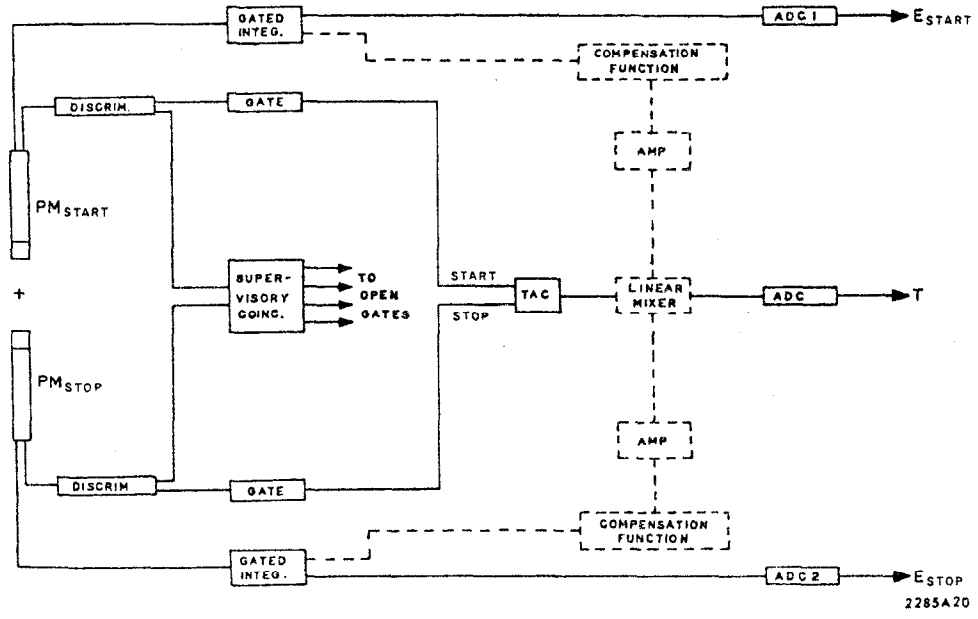

Figure 24. Block diagram of a time-interval measuring system with the time walk compensator shown in dashed lines (Ba 72).

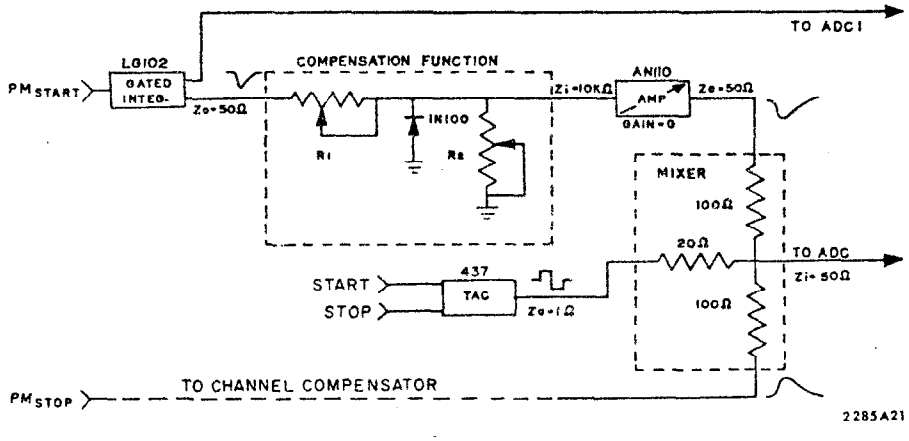

Figure 25. Circuit details of the compensation function and the linear mixer of Figure 24 (Ba 72).

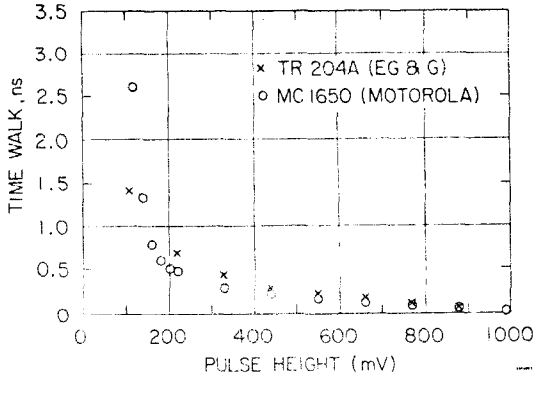

Figure 26. Time walk vs pulse height of two typical discriminators (Ba 73).